A new technique for finite element limit-analysis of Hill materials, with an application to the assessment of criteria for anisotropic plastic porous solids

Léo Morin, Komlanvi Madou, Jean-Baptiste Leblond, Djimédo Kondo

A new technique for finite element limit-analysis of Hill materials, with an application to the assessment of criteria for anisotropic plastic porous solids

Léo Morin *, Komlanvi Madou, Jean-Baptiste Leblond, Djimédo Kondo

Université Pierre-et-Marie-Curie, Institut d'Alembert, UMR 7190 CNRS, 4, place Jussieu, 75252 Paris cedex 05, France

Abstract

The present work is devoted to the numerical limit-analysis of Hill materials with particular emphasis on anisotropically plastic porous solids. Its aim is to provide an efficient method of limit-analysis based on the standard finite element method including elasticity, and present a few applications.

We first present the numerical implementation of Hill's criterion. We then describe the procedure used for the numerical limit-analysis, which basically consists of using a single large load step ensuring that the limit-load is reached, without updating the geometry. Also, the convergence of the elasto-plastic iterations is accelerated by suitably adjusting the elastic properties of the material.

The method is applied to assess Gurson-like criteria for orthotropically plastic materials containing spheroidal voids. This is done by performing numerical limit-analyses of elementary cells made of a Hill material and containing confocal spheroidal voids, subjected to classical conditions of homogeneous boundary strain rate. The numerical results are compared to the model predictions for both the yield surface and the flow rule, and this permits to discuss the accuracy of the theoretical models considered.

Key words: Numerical limit-analysis, Hill materials, Porous media, Cell calculations, Numerical assessment

1 Introduction

The most classical model of plastic porous solids, proposed by Gurson (1977), has been obtained by combining homogenization theory and limit-analysis of a spherical (or cylindrical) cell, made of a rigid-ideal-plastic von Mises material containing a spherical (or cylindrical) void, and loaded arbitrarily through conditions of homogeneous boundary strain rate.

* Corresponding author.

Owing to the intrinsic limitation of this model to isotropic materials containing spherical (or cylindrical) voids, several extensions were developed by accounting for void shape effects: Gologanu et al. (1993, 1994, 1997)'s model applies to isotropic materials containing spheroidal prolate or oblate voids [1] and is known as the *GLD model*. Some generalization of these works has been very recently proposed by Madou and Leblond (2012a,b) who consider a general ellipsoidal void embedded in a von Mises matrix.
Another type of extension of the Gurson model has consisted in the consideration of anisotropic Hill matrices (Hill, 1948) containing first spherical voids (Benzerga and Besson, 2001), then spheroidal ones (Monchiet et al., 2008). Later, Keralavarma and Benzerga (2010) investigated the same problem by considering a richer description of the velocity field.
The utility of the models just mentioned lies in the fact that non-spherical voids and plastically anisotropic matrices are quite common in practice.

All these criteria need to be critically assessed through numerical analyses of the representative cells considered in their derivation. While the criteria for isotropic von Mises matrices have already been widely assessed (Gologanu, 1997; Madou and Leblond, 2012b, 2013), those for anisotropic Hill matrices have been studied only in a partial way. Thus, Pastor et al. (2012) very recently provided numerical upper and lower bounds of the yield surfaces in the case of spherical and prolate spheroidal cavities, but no results were provided in this work about the flow rules associated to the yield surfaces.
In order to fully understand the effect of plastic anisotropy and void shape, it is necessary to complete Pastor et al. (2012)'s numerical results for spherical, cylindrical, spheroidal prolate and oblate voids embedded in a Hill material, by performing numerical limit-analyses of the representative cells considered. In the present work, we shall consider both the yield criterion and the macroscopic associated flow rule.
The assessment of the models dealing with orthotropic Hill matrices is particularly important given that they are based on a seemingly crude approximation: namely, they consider trial velocity fields identical to those commonly considered in the case of von Mises matrices. Thus, Benzerga and Besson (2001) used the same velocity fields as Gurson (1977), Monchiet et al. (2008) used those of Gologanu et al. (1993, 1994) and finally Keralavarma and Benzerga (2010) used the richer velocity fields of Gologanu et al. (1997).

Estimated solutions of a limit-analysis problem can be obtained by two complementary approaches providing approximate upper and lower bound solutions, known respectively as the *kinematic and static bounds*. These approaches require some minimization in the kinematic approach and some maximization in the static approach, which can only be achieved by numerical methods in general.
The first attempt to provide numerical solutions of limit-analysis problems was based on linear programming (Anderheggen and Knöpfel, 1972; Bottero et al., 1980) and the finite element method: the yield surface was approximately replaced by a polygonal surface, leading to a set of linear inequalities which were solved using linear programming. Both lower and upper bounds have been investigated (Sloan, 1988, 1989; Sloan and Kleeman, 1995). Despite the relatively simplicity of the method, this kind of approach introduces inherent source of inaccuracies in the approximation of the yield surface, and also requires

[1] Monchiet et al. (2013) used more sophisticated Eshelby-like velocity fields for the same kind of extension.

a specific implementation into a finite element code in order to solve the linear system.
Other significant contributions in the field of numerical limit-analysis were the so-called non linear programming methods (Capsoni and Corradi, 1997; Lyamin and Sloan, 2002a,b; Krabbenhoft and Damkilde, 2003). With these methods, the limit-analysis problem was directly solved without any linearisation, using non linear algorithms, for instance conic programming or interior point optimization. These works mainly considered isotropic materials governed by von Mises's criterion, and sometimes Drucker-Prager's criterion. Extensions to anisotropic criteria have also been proposed (Corradi et al., 2006; Pastor et al., 2012). These "non linear" methods lead to an estimation of the limit-load without introducing any approximation on the yield surface, but they require complex numerical developments for the optimization procedure.
Recently, Madou and Leblond (2012b) proposed a numerical method to solve limit-analysis problems for von Mises materials, based on the standard finite element method including elasticity, without introducing any approximation of the yield surface or supplementary optimization procedure.

The aim of this paper is to provide a new technique to solve limit-analysis problems for plastically anisotropic materials obeying Hill (1948)'s criterion, based on an extension of Madou and Leblond (2012b)'s procedure for isotropic material. The main advantages of the method proposed are that since it relies on the usual finite element method including elasticity, it requires only few developments, and benefits from the entire know-how developed for, and incorporated in standard codes. (The accuracy of the numerical results it provides has thus been established by Madou and Leblond (2012b), in the case of isotropic materials).
The method will be used to provide numerical results for anisotropic plastic porous materials. These results will be used to assess the models mentioned previously for anisotropic matrices containing spheroidal voids. They could also potentially be used to validate any similar yield criterion.

The paper is organized as follows :

- In Section 2, we first develop a numerical implementation of Hill's criterion and the associated flow rule into a finite element code, suggested by De Borst and Feenstra (1990), in which the sole unknown in the local projection algorithm is the plastic multiplier. A new finite element technique for numerical limit-analysis is then proposed. The principle of this technique consists of using this algorithm with a single large load step, without any geometry update. Also, the elastic properties of the material are suitably adjusted in order to accelerate the convergence of the global elasto-plastic iterations.
- Section 3 investigates the application of this technique to porous plastic materials obeying Hill's criterion. Spheroidal cells containing confocal spheroidal voids are subjected to conditions of homogeneous boundary strain rate. The numerical yield surfaces and flow rules are compared to those predicted by existing models in various cases. This permits to discuss the pertinence of the trial velocity fields used in the derivation of the models.

2 Finite element limit-analysis of Hill materials

2.1 Hill's criterion

The materials considered in this study are assumed to be rigid-plastic and obey Hill (1948)'s yield criterion which stands as an extension of von Mises's criterion taking account of the plastic anisotropy. With respect to the Cartesian coordinate system associated to the axes of orthotropy, the Hill criterion reads:

$$f(\boldsymbol{\sigma}) = \boldsymbol{\sigma} : \mathbb{A} : \boldsymbol{\sigma} - \sigma_0^2 = \sigma_{eq}^2 - \sigma_0^2 \leq 0 \tag{1}$$

where σ_{eq} is the Hill equivalent stress, σ_0 the "yield stress" and $\mathbb{A}$ an orthotropic fourth-order tensor satisfying both major and minor symmetries ($A_{ijkl} = A_{jikl} = A_{ijlk} = A_{klij}$). Employing a Voigt-type notation, such as used in finite elements codes, $\mathbb{A}$ and $\boldsymbol{\sigma}$ may be considered as a 6×6 matrix and a 6-vector, respectively:

$$\mathbb{A} \equiv \begin{pmatrix} A_{11} & A_{12} & A_{13} & 0 & 0 & 0 \\ A_{12} & A_{22} & A_{23} & 0 & 0 & 0 \\ A_{13} & A_{23} & A_{33} & 0 & 0 & 0 \\ 0 & 0 & 0 & A_{44} & 0 & 0 \\ 0 & 0 & 0 & 0 & A_{55} & 0 \\ 0 & 0 & 0 & 0 & 0 & A_{66} \end{pmatrix}; \qquad \boldsymbol{\sigma} \equiv \begin{pmatrix} \sigma_1 \equiv \sigma_{11} \\ \sigma_2 \equiv \sigma_{22} \\ \sigma_3 \equiv \sigma_{33} \\ \sigma_4 \equiv \sigma_{12} \\ \sigma_5 \equiv \sigma_{13} \\ \sigma_6 \equiv \sigma_{23} \end{pmatrix} \tag{2}$$

Note that the coefficients A_{ij} here verify the relations

$$\sum_i A_{1i} = \sum_i A_{2i} = \sum_i A_{3i} = 0 \tag{3}$$

arising from invariance of the criterion upon addition of a hydrostatic stress.

2.2 Numerical implementation of the Hill criterion

In order to perform numerical limit-analyses, we first need an efficient finite element implementation of Hill materials. Only the "local" step is considered here, because the "global" step does not depend on the yield criterion and is standard in finite element codes. Furthermore, the application of the algorithm is limited to limit-analysis so it is presented in the context of small strains and ideal plasticity; its extension to large strains and strain-hardening materials can be achieved without any specific difficulty.

Let us develop the local projection algorithm suggested by De Borst and Feenstra (1990) for the Hill criterion. This algorithm considers the plastic multiplier as the unique unknown of the projection problem. That this is possible is due, as will be seen, to the quadratic form of the criterion, even though the property of collinearity of the stress deviators before and after the plastic correction, which is well-known for von Mises's criterion, is lost for Hill's criterion. The fact that the problem may be reduced to finding a single unknown permits a faster procedure of solution, thanks to an easier convergence of the necessary Newton iterations.

The equations of the local elastoplasticity problem are as follows:

Decomposition of the total strain: $\boldsymbol{\epsilon} = \boldsymbol{\epsilon}^e + \boldsymbol{\epsilon}^p$

Elasticity law: $\boldsymbol{\sigma} = \mathbb{C} : \boldsymbol{\epsilon}^e$

Hill's criterion: $f(\boldsymbol{\sigma}) = \sigma_{eq}^2 - \sigma_0^2 \leq 0$

Flow rule and consistency conditions: $\dot{\boldsymbol{\epsilon}}^p = \dot{\lambda}\frac{\partial f}{\partial \boldsymbol{\sigma}}(\boldsymbol{\sigma})$, $\dot{\lambda} \geq 0$, $\dot{\lambda} f(\boldsymbol{\sigma}) = 0$

where $\boldsymbol{\epsilon}^e$ is the elastic strain tensor, $\boldsymbol{\epsilon}^p$ the plastic strain tensor, $\mathbb{C}$ the stiffness tensor and $\dot{\lambda}$ the plastic multiplier.

The problem consists in finding the mechanical state $\mathcal{S}_{n+1} = \{\boldsymbol{\epsilon}_{n+1}, \boldsymbol{\epsilon}^p_{n+1}, \boldsymbol{\sigma}_{n+1}\}$ at time t_{n+1} resulting from a given strain increment $\Delta\boldsymbol{\epsilon}_n$, knowing the previous mechanical state $\mathcal{S}_n = \{\boldsymbol{\epsilon}_n, \boldsymbol{\epsilon}^p_n, \boldsymbol{\sigma}_n\}$ at time t_n. (The value of $\Delta\boldsymbol{\epsilon}_n$ is determined by the global step).

The flow rule is discretized using an implicit scheme. Since the material belongs to the category of generalized standard materials (see Son (1977); Halphen and Nguyen (1975)), the choice of such a scheme is relevant, because the local projection problem reduces, for such materials, to finding the minimum of a strictly convex function, which implies existence and uniqueness of the solution. The discretized flow rule then reads:

$$\Delta\boldsymbol{\epsilon}^p_n = \boldsymbol{\epsilon}^p_{n+1} - \boldsymbol{\epsilon}^p_n = \Delta\lambda_n \frac{\partial f}{\partial \boldsymbol{\sigma}}(\boldsymbol{\sigma}_{n+1}) \tag{4}$$

Using Voigt's notations, the above set of equations becomes:

$$\begin{aligned}
\boldsymbol{\sigma}_{n+1} &= \mathbb{C}.\boldsymbol{\epsilon}^e_{n+1} = \boldsymbol{\sigma}_n + \mathbb{C}.(\Delta\boldsymbol{\epsilon}_n - \Delta\boldsymbol{\epsilon}^p_n) \\
&= \boldsymbol{\sigma}^{elas}_{n+1} - \mathbb{C}.\Delta\boldsymbol{\epsilon}^p_n \quad , \qquad \boldsymbol{\sigma}^{elas}_{n+1} = \boldsymbol{\sigma}_n + \mathbb{C}.\Delta\boldsymbol{\epsilon}_n && (5)\\
\sigma^2_{n+1,eq} - \sigma_0^2 &\leq 0 && (6)\\
\Delta\boldsymbol{\epsilon}^p_n &= 2\Delta\lambda_n \mathbb{A}.\boldsymbol{\sigma}_{n+1} && (7)\\
\Delta\lambda_n(\sigma^2_{n+1,eq} - \sigma_0^2) &= 0. && (8)
\end{aligned}$$

In these equations $\boldsymbol{\sigma}^{elas}_{n+1}$ denotes the elastic predictor, that is the stress tensor resulting from the strain increment $\Delta\boldsymbol{\epsilon}_n$ fictitiously considered as purely elastic. To solve these

equations, two cases must be considered.

Elastic evolution If $f(\boldsymbol{\sigma}_{n+1}^{elas}) \leq 0$, then the evolution is purely elastic. The final state is given by:

$$\boldsymbol{\sigma}_{n+1} = \boldsymbol{\sigma}_{n+1}^{elas} \tag{9}$$
$$\boldsymbol{\epsilon}_{n+1}^{p} = \boldsymbol{\epsilon}_{n}^{p} \tag{10}$$

Elasto-plastic evolution If $f(\boldsymbol{\sigma}_{n+1}^{elas}) > 0$, then the elastic predictor is not plastically admissible. We need to add a plastic correction, given that the final stress must be such that $f(\boldsymbol{\sigma}_{n+1}) = 0$. The main difficulty is the determination of the plastic multiplier. Let us rewrite $\boldsymbol{\sigma}_{n+1}$ as

$$\begin{aligned}\boldsymbol{\sigma}_{n+1} &= \boldsymbol{\sigma}_{n+1}^{elas} - \mathbb{C}.\Delta\boldsymbol{\epsilon}_{n}^{p} \\ &= \boldsymbol{\sigma}_{n+1}^{elas} - \mathbb{C}.(2\Delta\lambda_n\mathbb{A}.\boldsymbol{\sigma}_{n+1}) \\ &= \boldsymbol{\sigma}_{n+1}^{elas} - 2\Delta\lambda_n\mathbb{C}.\mathbb{A}.\boldsymbol{\sigma}_{n+1}\end{aligned}$$

This implies that:

$$\boldsymbol{\sigma}_{n+1} = (\mathbb{I} + 2\Delta\lambda_n\mathbb{C}.\mathbb{A})^{-1}.\boldsymbol{\sigma}_{n+1}^{elas} \tag{11}$$

Equation (11) shows that with Hill's criterion instead of that of von Mises, the classical property of collinearity of $\boldsymbol{\sigma}_{n+1}$ and $\boldsymbol{\sigma}_{n+1}^{elas}$ is lost; however an explicit relation still exists between them as a direct consequence of the quadratic form of the criterion, leading to the possible reduction of the problem to finding the value of a single unknown. Indeed, the criterion $f(\boldsymbol{\sigma}_{n+1}) = 0$ then implies that:

$$[(\mathbb{I} + 2\Delta\lambda_n\mathbb{C}.\mathbb{A})^{-1}.\boldsymbol{\sigma}_{n+1}^{elas}].\mathbb{A}.[(\mathbb{I} + 2\Delta\lambda_n\mathbb{C}.\mathbb{A})^{-1}.\boldsymbol{\sigma}_{n+1}^{elas}] - \sigma_0^2 = 0 \tag{12}$$

which is an equation on the sole unknown $\Delta\lambda_n$. This non-linear equation may be solved by a Newton method. Once $\Delta\lambda_n$ is determined, one can easily compute the final stress $\boldsymbol{\sigma}_{n+1}$ using equation (11) and then the increment of plastic strain $\Delta\boldsymbol{\epsilon}_{n}^{p}$ using equation (7).

In practice, in order to accelerate convergence of the iterations, the initial value of $\Delta\lambda_n$ is not taken nil but equal to that value $\Delta\lambda_n^0$ corresponding to some isotropic material: $\Delta\lambda_n^0 = \frac{\sigma_0^2}{6\mu}(\frac{\sigma_{eq,VM}^{elas}}{\sigma_{eq,VM}} - 1)$, $\sigma_{eq,VM}$ denoting the von Mises equivalent stress, and μ the elastic shear modulus.

The global step of the elastoplasticity problem is achieved using a BFGS algorithm. It would also be possible to determine and use the consistent tangent operator, but in

practice, the convergence of the global elastoplastic iterations requires less CPU time with a BFGS algorithm.

The local projection algorithm just expounded has been implemented in the commercial finite element code SYSTUS® developed by ESI Group.

2.3 Numerical limit-analysis: principles

In order to numerically solve a limit-analysis problem for a Hill material, we will extend Madou and Leblond (2012b)'s procedure initially proposed for von Mises matrices. Thus, the limit-analysis problem will be solved using standard finite element simulations, by imposing a single large step, with no update of the geometry since geometric changes are disregarded in limit-analysis. The use of a large step instead of several small ones will permit faster calculations without introducing any error of principle: indeed in the following we show the equivalence of the equations of the time-discretized finite element problem and those of limit-analysis under such conditions.

The equations of limit-analysis of a structure Ω reduce to those of a problem of plasticity without elasticity in the small strain (linearized) context:

$$\begin{cases} \text{div } \boldsymbol{\sigma} = 0 \\ \mathbf{d} = \frac{1}{2}\left[\nabla_{\mathbf{X}}\mathbf{v} + (\nabla_{\mathbf{X}}\mathbf{v})^T\right] \\ f(\boldsymbol{\sigma}) \leq 0 \\ \mathbf{d} = \dot{\lambda}\dfrac{\partial f}{\partial \boldsymbol{\sigma}}(\boldsymbol{\sigma}), \quad \dot{\lambda} \geq 0, \quad \dot{\lambda} f(\boldsymbol{\sigma}) = 0 \end{cases} \quad \text{in } \Omega \qquad (13)$$

+B.C.

In these equations $\mathbf{X}$ denotes the position-vector in the initial configuration, $\mathbf{v}$ the velocity, $\mathbf{d}$ the strain rate, $\boldsymbol{\sigma}$ the Cauchy stress tensor, $f(\boldsymbol{\sigma})$ the Hill yield function, $\dot{\lambda}$ the plastic multiplier, and "B.C." stands for "boundary conditions".

Let us assume now that the elastoplastic problem is solved by the finite element method using an implicit algorithm for the local projection problem, with no update of the geometry and a single large step. Let $\boldsymbol{\sigma}^0 = \mathbf{0}$, $\boldsymbol{\sigma}^1$, $\mathbf{u}^0 = \mathbf{0}$, $\mathbf{u}^1$, $\boldsymbol{\epsilon}^0 = \mathbf{0}$, $\boldsymbol{\epsilon}^1$ denote the initial and final stresses, initial and final displacements, initial and final strains, respectively. If we make sure that plastic strains are generally much bigger than elastic strains, by adopting

a large load increment, then the discretized equations read:

$$\left\{\begin{array}{ll} \text{div } \boldsymbol{\sigma}^1 & = 0 \\ \boldsymbol{\epsilon}^1 & = \frac{1}{2}\left\{\nabla_{\mathbf{X}}(\mathbf{u}^1) + [\nabla_{\mathbf{X}}(\mathbf{u}^1)]^T\right\} \\ f\left(\boldsymbol{\sigma}^1\right) & \leq 0 \\ \boldsymbol{\epsilon}^1 - \boldsymbol{\epsilon}^0 = \boldsymbol{\epsilon}^1 & \simeq \Delta\lambda \dfrac{\partial f}{\partial \boldsymbol{\sigma}}\left(\boldsymbol{\sigma}^1\right), \quad \Delta\lambda \geq 0, \quad \Delta\lambda f(\boldsymbol{\sigma}^1) = 0 \end{array}\right. \quad \text{in } \Omega \qquad (14)$$

+B.C.

where $\Delta\lambda$ denotes the discretized plastic multiplier. The equivalence of systems (13) and (14) is clear, with the correspondences $\boldsymbol{\sigma} \leftrightarrow \boldsymbol{\sigma}^1$, $\mathbf{v} \leftrightarrow \mathbf{u}^1$, $\mathbf{d} \leftrightarrow \boldsymbol{\epsilon}^1$. Note that the keypoint here is that $\frac{\partial f}{\partial \boldsymbol{\sigma}}$ is taken at the point $\boldsymbol{\sigma}^1$ rather than $\boldsymbol{\sigma}^0 = \mathbf{0}$ in the discretized flow rule, as a result of the use of an implicit algorithm.

The conclusion is that the problem of limit-analysis may be solved by the standard finite element method including elasticity, with a single load step sufficiently large to ensure that the elastic strains in the structure are generally much smaller than the plastic strains.

2.4 Numerical limit-analysis: special case of a completely plastic structure

In this section we present a method of adjustment of the elastic properties for a Hill material in the finite element problem which permits, under certain conditions, to reduce the load step, and thus accelerate convergence of the elastoplastic iterations.

Indeed, let us consider *the special, but frequent case of a structure which is entirely plastic when its limit-load is reached*. Equations $(13)_{3,4,5}$ of the limit-analysis problem then read:

$$\left\{\begin{array}{ll} f\left(\boldsymbol{\sigma}\right) = 0 & \\ \mathbf{d} \quad = \dot{\lambda} \dfrac{\partial f}{\partial \boldsymbol{\sigma}}\left(\boldsymbol{\sigma}\right) = 2\dot{\lambda}\mathbb{A}.\boldsymbol{\sigma}, & \dot{\lambda} > 0 \end{array}\right. \quad \text{in } \Omega \qquad (15)$$

Let us now suppose that the elastoplastic problem is solved by the finite element method, considering a quasi-incompressible anisotropic elastic material whose compliance tensor $\mathbb{D} = \mathbb{C}^{-1}$ is proportional to Hill's tensor $\mathbb{A}$:

$$\mathbb{D} \approx \alpha\mathbb{A}, \quad \alpha > 0 \qquad (16)$$

(In practice, diagonal terms of $\mathbb{D}$ are slightly enhanced to avoid exact incompressibility which would lead to numerical difficulties). This is possible because limit-loads are known to be independent of elastic coefficients. In practice, the coefficient α may be adjusted in such a way that the components of $\mathbb{D}$ be of order $1/E$, where E is Young's modulus.

Assume that the problem is solved using a single step *sufficiently large to ensure that the limit-load is reached, but not necessarily that the final elastic strain* $\boldsymbol{\epsilon}^{e1}$ *is much smaller than the final plastic strain* $\boldsymbol{\epsilon}^{p1}$. Under such conditions, $\boldsymbol{\epsilon}^{e1} = \mathbb{D}.\boldsymbol{\sigma}^1 \approx \alpha\mathbb{A}.\boldsymbol{\sigma}^1$, so equations $(14)_{3,4,5}$ of the discretized problem become:

$$\begin{cases} f\left(\boldsymbol{\sigma}^1\right) = 0 \\ \boldsymbol{\epsilon}^1 - \boldsymbol{\epsilon}^0 = \boldsymbol{\epsilon}^1 = \boldsymbol{\epsilon}^{e1} + \boldsymbol{\epsilon}^{p1} \approx \alpha\mathbb{A}.\boldsymbol{\sigma}^1 + \Delta\lambda \frac{\partial f}{\partial \boldsymbol{\sigma}}\left(\boldsymbol{\sigma}^1\right) \quad \text{in } \Omega. \\ \qquad\qquad\qquad\qquad = \left(\alpha + 2\Delta\lambda\right)\mathbb{A}.\boldsymbol{\sigma}^1 \end{cases} \tag{17}$$

The term $(\alpha + 2\Delta\lambda)$ here is positive since both α and $\Delta\lambda$ are positive. It follows that a solution of the finite element equations $(14)_{1,2,6}$ - (17) is also a solution of the equations $(13)_{1,2,6}$ - (15) of the theoretical problem, with the same correspondences $\boldsymbol{\sigma} \leftrightarrow \boldsymbol{\sigma}^1$, $\mathbf{v} \leftrightarrow \mathbf{u}^1$, $\mathbf{d} \leftrightarrow \boldsymbol{\epsilon}^1$ as before.

Note that this equivalence of solutions holds only for an entirely plastic structure: if the structure is only partially plastic, then there are points where $\dot{\lambda} = 0$ but $\alpha + 2\Delta\lambda = \alpha > 0$, so that the correspondence between the theoretical and numerical flow rules is imperfect.

Thus, if the structure is entirely plastic when its limit-load is reached, a finite element solution of the problem of limit-analysis may be obtained by considering an elastoplastic material whose elastic compliance tensor is proportional to Hill's anisotropic tensor, combined with a single, moderately large loading step ensuring that the limit-load is reached but not necessarily that the elastic strain is generally negligible.

3 Numerical yield surfaces and directions of plastic flow of anisotropic plastic porous materials

3.1 Generalities

We consider spheroidal cells containing a confocal spheroidal void and subjected to conditions of homogeneous boundary strain (Mandel, 1964; Hill, 1967):

$$\mathbf{u}(\mathbf{X}) = \mathbf{E}.\mathbf{X} \qquad \text{on } \partial\Omega \tag{18}$$

where $\mathbf{u}$ is the displacement, $\mathbf{X}$ the initial position-vector, $\mathbf{E}$ the overall strain tensor and $\partial\Omega$ the external boundary of the cell Ω. Attention is restricted to overall strain tensors having principal directions identical to those of the ellipsoidal cell, implying existence of symmetries about three perpendicular planes which permit to mesh only 1/8 of the structure.

The meshes used are represented in Figures 1a, 1b and 1c, respectively for a sphere,

an oblate and a prolate spheroid: they consist of 26,481 nodes and 24,000 selectively subintegrated trilinear 8-node brick elements, and there are 20 elements in the radial direction. The mesh used for the cylindrical void, represented on Figure 1d, consists of 9,920 nodes and 4,800 selectively subintegrated trilinear 8-node brick elements, and there are 30 elements in the radial direction. The values of the macroscopic strain components imposed vary from roughly 0.1 to 1, requiring a few hundreds of BFGS iterations in order to warrant good convergence of the global elastoplastic iterations.

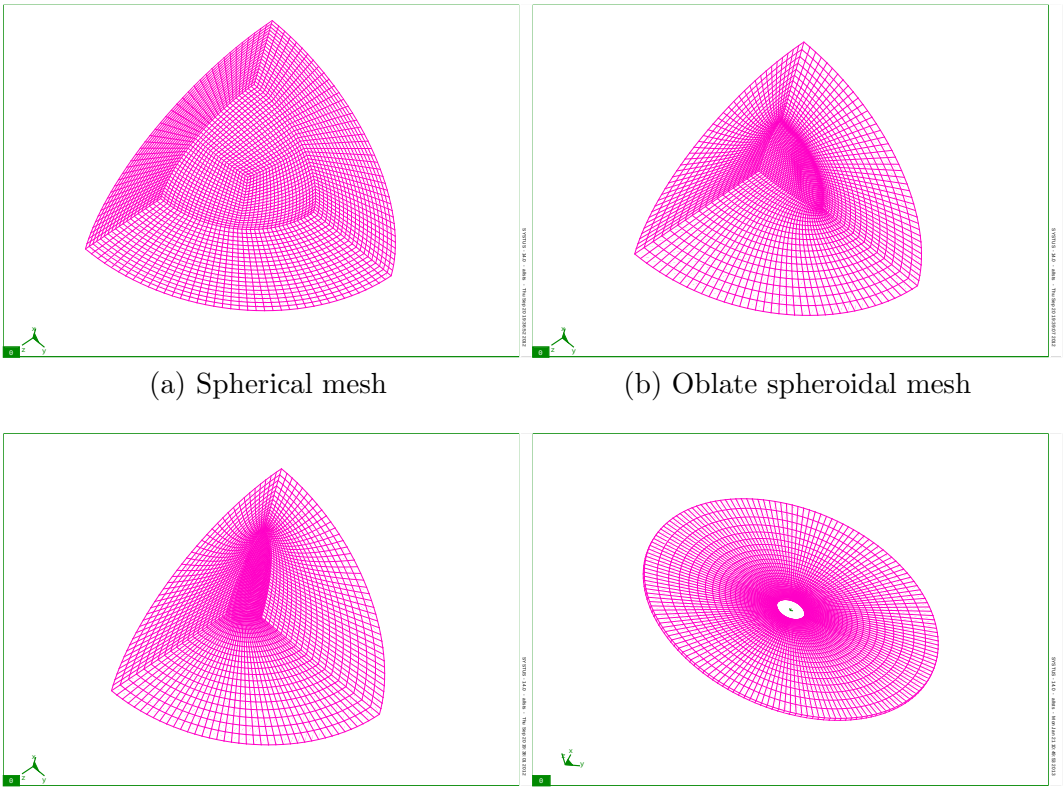

(a) Spherical mesh (b) Oblate spheroidal mesh

(c) Prolate spheroidal mesh (d) Cylindrical mesh

Fig. 1. Meshes used for micromechanical simulations

As mentioned before, the calculations use the SYSTUS® finite element code developed by ESI Group; this code allows the user to write higher level programmes, in order to manage and exploit the calculations. Three programmes have been developed:

- The first one creates the mesh: it displaces nodes of a standardly meshed hollow sphere so as to obtain a spheroid containing a spheroidal void.
- The second programme runs the calculations. The principal components of the overall strain tensor are adjusted using a Newton method, in order to match the desired values of the ratios of the overall stress components.
- Finally, the third programme exploits the results obtained by calculating the overall stress tensor through a volume average of the local one:

$$\boldsymbol{\Sigma} = \frac{1}{\mathrm{vol}(\Omega)} \int_{\Omega-\omega} \boldsymbol{\sigma} dV \tag{19}$$

where ω is the volume of the void and $\Omega - \omega$ the domain occupied by the solid matrix.

3.2 Material constants and quantities investigated

Numerical studies of anisotropic plastic porous materials and comparisons with theoretical criteria proposed by Benzerga and Besson (2001), Monchiet et al. (2008) and Keralavarma and Benzerga (2010) are performed by considering an anisotropic aluminium alloy whose material parameters are taken from Benzerga (2000). In Table 1 are reported the values of the components of the tensor $\mathbb{A}$ appearing in the definition (2) of the Hill criterion, together with those of a von Mises material for comparison. Note the very important anisotropy of the shear coefficients A_{44} and A_{55}.

Material	A_{11}	A_{22}	A_{33}	A_{12}	A_{13}	A_{23}	A_{44}	A_{55}	A_{66}
Isotropic	1	1	1	-0.5	-0.5	-0.5	3	3	3
Anisotropic	0.9855	0.87	0.921	-0.4673	-0.5182	-0.4028	10.494	10.8675	3.288

Table 1
Values of Hill's anisotropy coefficients

The spheroid's axis of rotational symmetry is denoted Ox_3. Axisymmetric loadings ($\Sigma_{11} = \Sigma_{22} \neq 0$, $\Sigma_{33} \neq 0$, other $\Sigma_{ij} = 0$) are considered in all numerical tests.

Two complementary aspects are investigated in these studies. First, we compare the yield surfaces provided by the analytical models to those obtained numerically. These yield surfaces are represented in a plane $(\frac{\Sigma_m}{\sigma_0}, \frac{\Sigma_{33}-\Sigma_{11}}{\sigma_0})$, where $\Sigma_m = \frac{1}{3}(\Sigma_{11} + \Sigma_{22} + \Sigma_{33})$ is the mean stress.

A second aspect concerns the comparison of the macroscopic flow directions represented by the ratios $\frac{D_{11}}{D_{22}}$,$\frac{D_{11}}{D_{33}}$ and $\frac{D_{22}}{D_{33}}$. The numerical macroscopic strains E_{11}, E_{22}, E_{33} resulting from the boundary conditions may be identified to the components of the *true* macroscopic strain rates D_{11}, D_{22}, D_{33}, using the correspondence between the equations of limit-analysis and those of the finite element problem established in Section 2.3. The *approximate* analytical macroscopic strain rate tensor is deduced up to some unimportant positive multiplicative constant, from the normality of the flow rule:

$$\mathbf{D} = \dot{\lambda}\frac{\partial \Phi}{\partial \boldsymbol{\sigma}}(\boldsymbol{\sigma}) \tag{20}$$

where $\Phi(\boldsymbol{\sigma})$ denotes the theoretical macroscopic yield criterion investigated (see Appendix A). More precisely, $(\mathbf{e}_1, \mathbf{e}_2)$ denoting some orthogonal basis of the Euclidian plane, we shall consider the vector $D_{11}\mathbf{e}_1 + D_{22}\mathbf{e}_2$ and study the angle ϕ_{12} it makes with the vector $\mathbf{e}_1$, as a function of an angle ψ measuring the position of the stress tensor considered on the yield surface; see Figures 2a and 2b. We shall also study some angles ϕ_{13} and ϕ_{23} defined similarly, as functions of the same angle ψ.

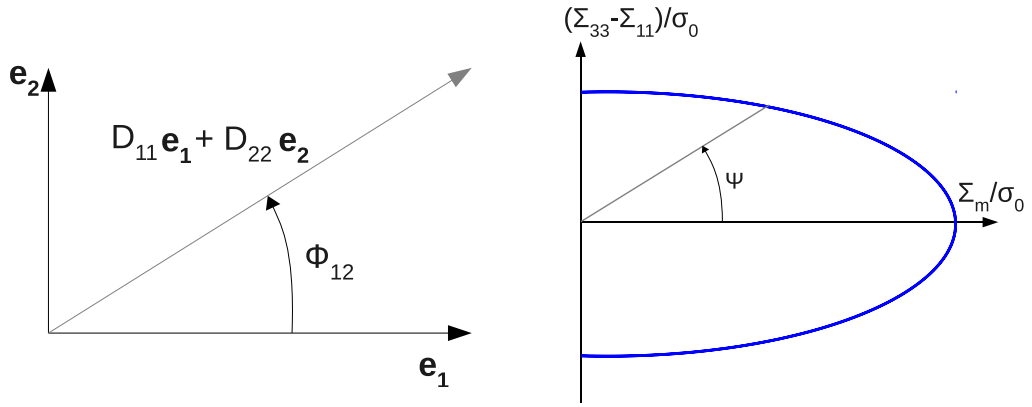

(a) Definition of the angle ϕ_{12} (b) Definition of the angle ψ

Fig. 2. Definition of angles

3.3 Spherical voids

We first investigate the case of a spherical void embedded in a spherical cell. A fixed porosity of $f = 10^{-2}$ is considered; this is a typical value for ductile metals, once nucleation of voids has taken place.

In this case, the numerical yield surface, shown on Figure 3a, is in agreement with the theoretical one proposed by Benzerga and Besson (2001) and Monchiet et al. (2008). The comparison with Gurson (1977)'s criterion for the same void but in an isotropic matrix clearly shows the effect of anisotropy and the ability of the anisotropic criterion proposed to capture it.

With regards to the flow rule, the results are plotted in Figures 3b, 3c and 3d. Again, a remarkable agreement is noted between numerical results and theoretical predictions, except for ϕ_{12} near $\psi = 0$ which corresponds to a hydrostatic stress state ($\Sigma_{11} = \Sigma_{22} = \Sigma_{33}$): there is a difference of about 30° between the numerical results and the prediction of the model.

Complementary results are provided for a spherical void embedded in a spherical cell with a porosity $f = 10^{-1}$. The yield surface is plotted in Figure 4a, and the angles ϕ_{12}, ϕ_{13} and ϕ_{23} in Figures 4b, 4c and 4d. Again, a good agreement is observed between numerical and theoretical yield surfaces. Also, the flow rule is well reproduced except near the hydrostatic point for the angle ϕ_{12}.

3.4 Prolate voids

We now consider the case of a prolate spheroidal void, with axes in the proportions $(1 : 1 : 5)$. A fixed of porosity of 10^{-2} is considered.

The numerical results for the yield surface are shown in Fig. 5a. In this case, Monchiet

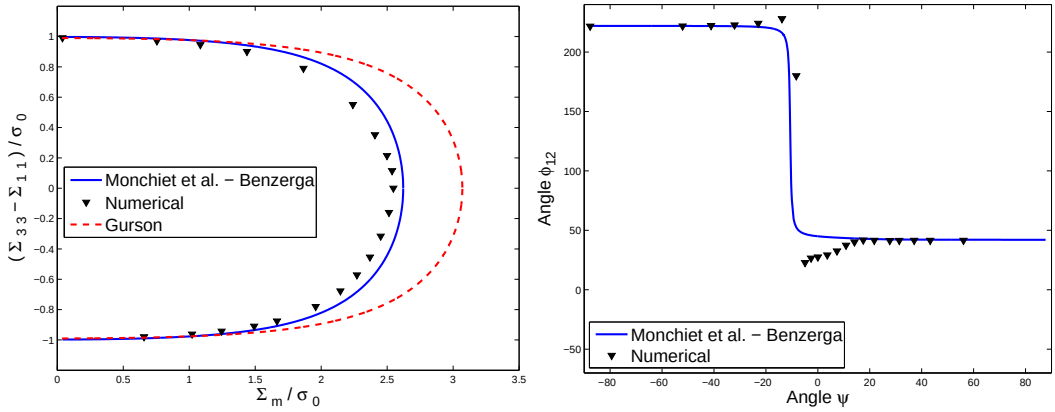

(a) Yield surface

(b) Flow rule : angle ϕ_{12}

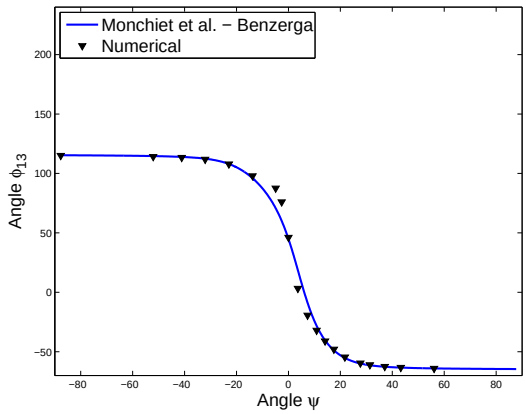

(c) Flow rule : angle ϕ_{13}

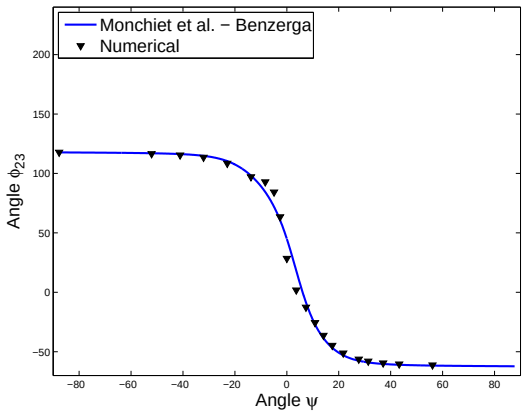

(d) Flow rule : angle ϕ_{23}

Fig. 3. Numerical results for a spherical void: porosity 10^{-2}

et al. (2008)'s and Keralavarma and Benzerga (2010)'s criteria appear to be very close and in very good agreement with the numerical data. Note however that the criterion proposed by Monchiet et al. (2008) is slightly better. Theoretical results corresponding to Gologanu et al. (1997)'s criterion for the same prolate void in an isotropic matrix, and to that of Gurson (1977) for a spherical void in an isotropic matrix, are also plotted to highlight the combined effects of plastic anisotropy and void shape: these effects are of the same order.

Also, the analytical flow rules (Figures 5b, 5c, 5d) accurately represent the numerical data, even near the hydrostatic point.

To supplement these results, we consider a cylindrical void, which is a special case of a prolate spheroidal one. For this particular geometry, Monchiet et al. (2008)'s and Keralavarma and Benzerga (2010)'s criteria coincide and reduce to that obtained previously by Benzerga and Besson (2001). Although a moderate discrepancy between the analytical and numerical points is observed for the yield surface (Figure 6a), the comparison with Gurson's model for cylindrical voids shows that Monchiet et al. (2008)'s and Keralavarma and Benzerga (2010)'s criterion essentially captures the effect of anisotropy. Furthermore, the theoretical model is very accurate for the flow rule (Figures 6b, 6c, 6d).

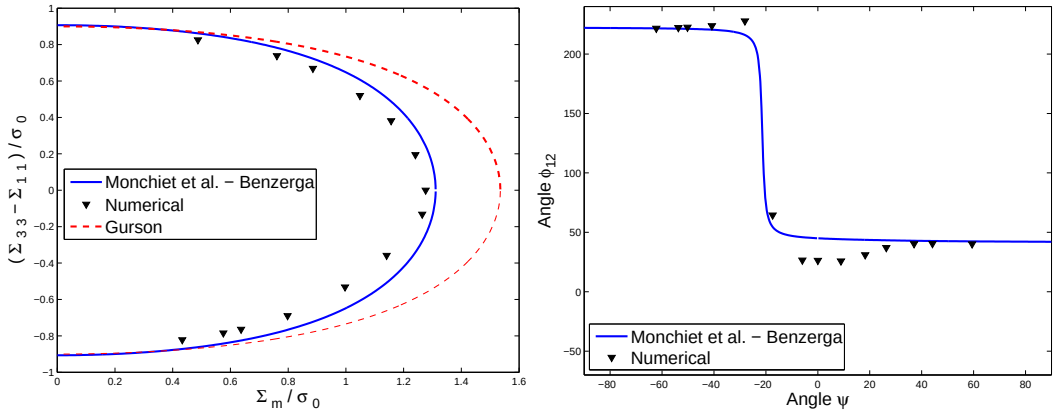

(a) Yield surface

(b) Flow rule : angle ϕ_{12}

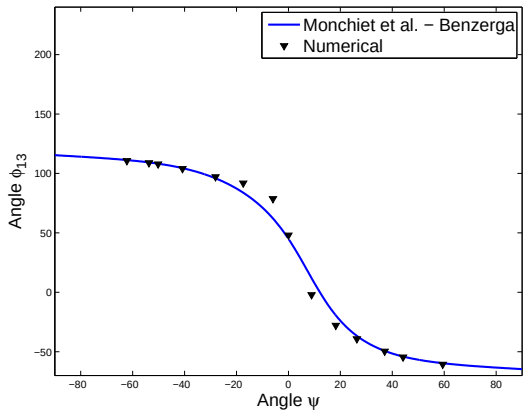

(c) Flow rule : angle ϕ_{13}

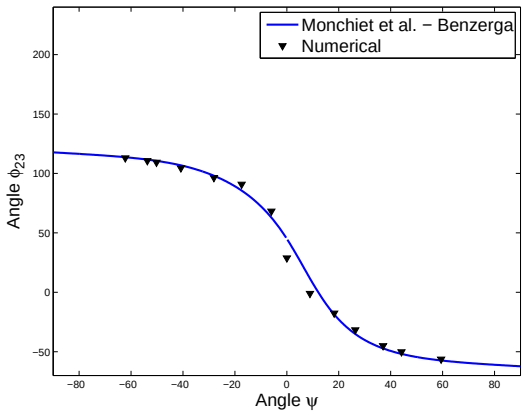

(d) Flow rule : angle ϕ_{23}

Fig. 4. Numerical results for a spherical void: porosity 10^{-1}

3.5 Oblate voids

We finally investigate the case of an oblate spheroidal void, with axes in the proportions $(5:5:1)$ and a porosity of 10^{-2}.

In this case, the theoretical results for the yield locus are still very good, particularly for Keralavarma and Benzerga (2010)'s criterion which appears to be closer to the numerical one than that of Monchiet et al. (2008) (Figure 7a). For completeness, the theoretical results corresponding to Gologanu et al. (1997)'s criterion for the same oblate void in an isotropic matrix, and to that of Gurson (1977) for a spherical void in an isotropic matrix, are also provided in order to show the effects of matrix anisotropy and void shape: again, these effects are of the same order.

With regards to the flow rule, there are only minor differences between the two theoretical predictions and they are both in very good agreement with the numerical results.

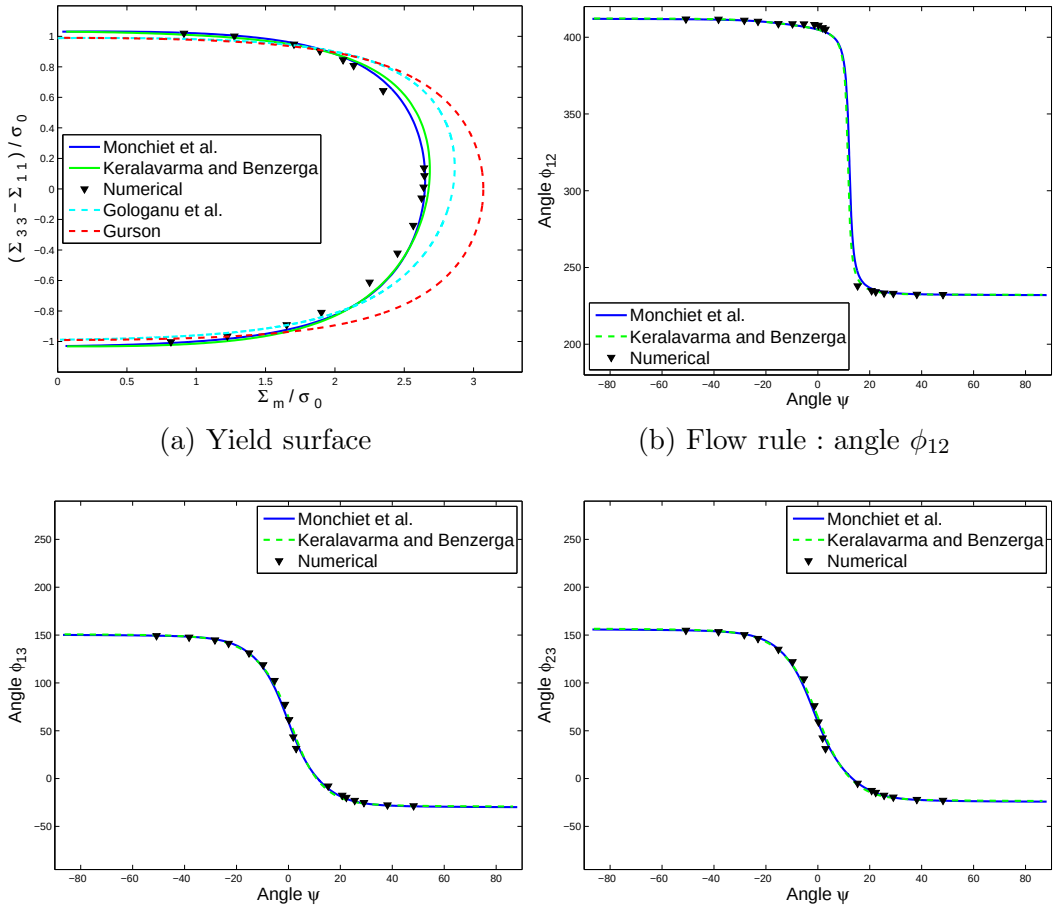

(a) Yield surface

(b) Flow rule : angle ϕ_{12}

(c) Flow rule : angle ϕ_{13}

(d) Flow rule : angle ϕ_{23}

Fig. 5. Numerical results for a prolate void: porosity 10^{-2}

3.6 Discussion

In the cases considered (spherical, prolate spheroidal, oblate spheroidal and cylindrical voids), the anisotropic criteria of Benzerga and Besson (2001), Monchiet et al. (2008) and Keralavarma and Benzerga (2010), are very close to the numerical results resulting from limit-analysis performed by the finite element method, for both the yield surfaces and the directions of plastic flow. Comparisons with Gurson (1977)'s and Gologanu et al. (1997)'s criteria show a complex coupling between material anisotropy and void shape, which is well reproduced by the anisotropic criteria considered.

Since the theoretical criteria were obtained by using trial velocity fields corresponding to a plastically *isotropic* matrix, the above results emphasize the great interest of this class of velocity fields even when considering *anisotropic* matrices. The success of the "isotropic" velocity fields may be explained by the variational characterization of the overall yield locus in terms of the overall plastic dissipation: indeed, provided that the anisotropy is not too great, using a trial "isotropic" velocity field differing modestly from the exact "anisotropic" one in the approximate limit-analysis must lead to a reasonable estimate of the minimum of the plastic dissipation, leading itself to a good estimate of the yield locus.

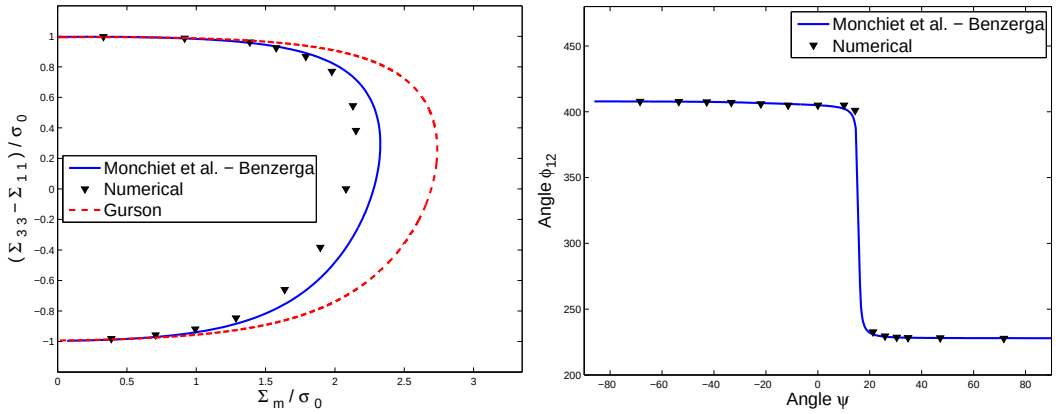

(a) Yield surface

(b) Flow rule : angle ϕ_{12}

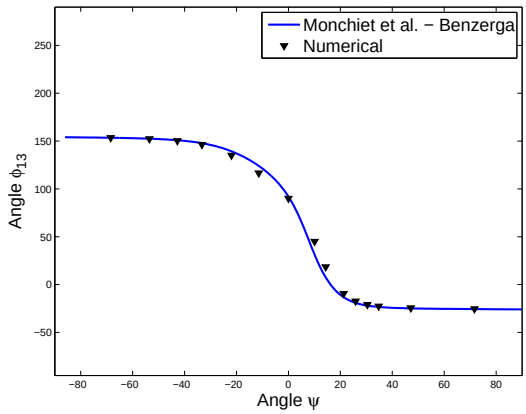

(c) Flow rule : angle ϕ_{13}

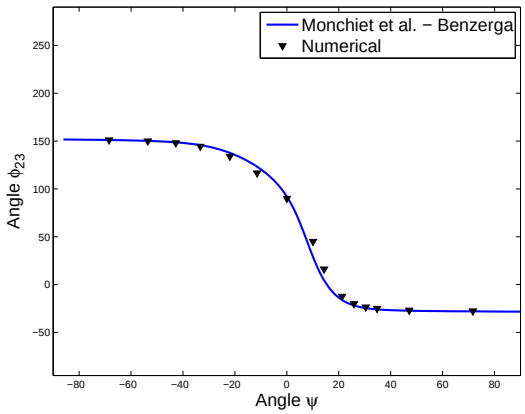

(d) Flow rule : angle ϕ_{23}

Fig. 6. Numerical results for a cylindrical void: porosity 10^{-2}

4 Conclusion

In this paper, we presented a new finite element technique for numerical limit-analysis of Hill materials. This method, unlike other ones, does not require any approximation of the yield surface or extra optimization procedure: it is based on the standard finite element method including elasticity. The equations of the time-discretized finite element problem reduce to those of limit-analysis by imposing a single large load step, with no geometry update, and using an implicit algorithm for the local projection procedure. The convergence of the elastoplastic iterations is accelerated by using an elastic compliance of the material proportional to Hill's tensor: this permits to use a moderate load step, provided that the structure is entirely plastic when its limit-load is reached.

This new technique was then applied to the study of the overall criteria of anisotropic plastic porous solids. We performed numerical limit-analyses of spheroidal cells containing confocal spheroidal voids and made of Hill materials, subjected to conditions of homogeneous boundary strain rate. The results were compared to available theoretical anisotropic criteria (Benzerga and Besson (2001), Monchiet et al. (2008) and Keralavarma and Benzerga (2010)) for spherical, prolate and oblate spheroidal voids, in order to assess their accuracy. Both theoretical yield surfaces and directions of plastic flow appeared to be in

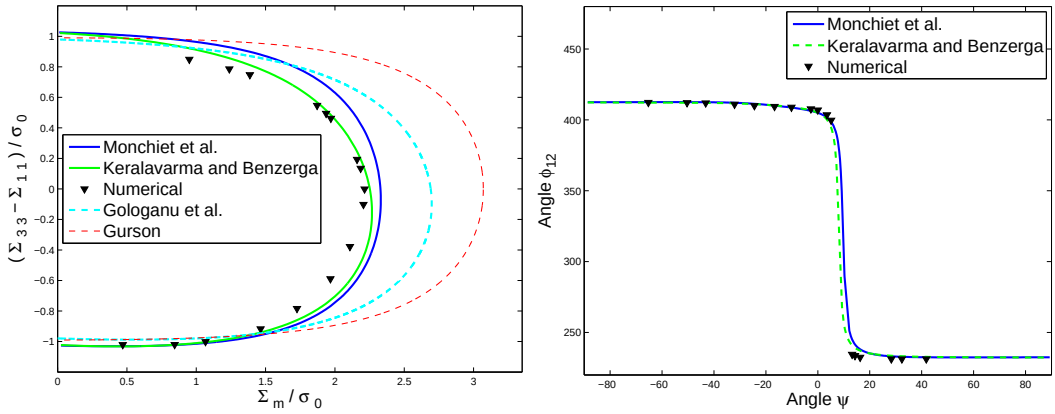

(a) Yield surface

(b) Flow rule : angle ϕ_{12}

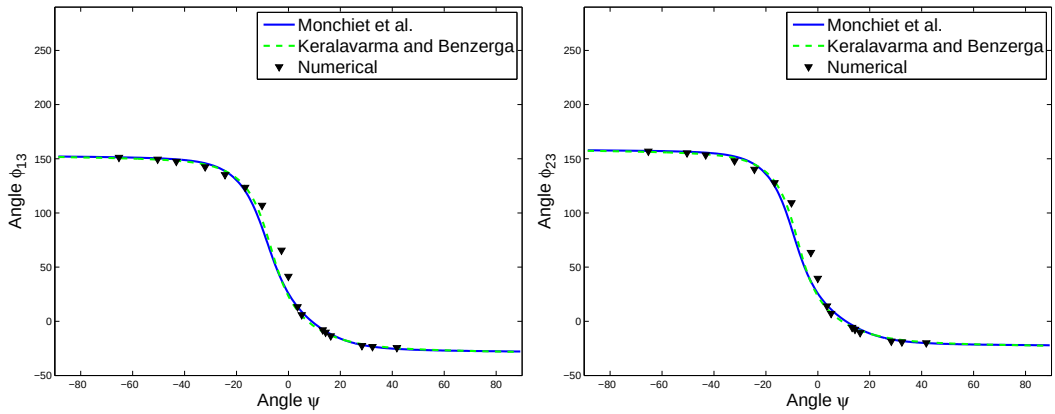

(c) Flow rule : angle ϕ_{13}

(d) Flow rule : angle ϕ_{23}

Fig. 7. Numerical results for a oblate void: porosity 10^{-2}

very good agreement with the numerical ones, except near the hydrostatic point where some discrepancies were observed for the flow rule in some cases. Keralavarma and Benzerga (2010)'s criterion was noted to give slightly better results than that Monchiet et al. (2008)'s criterion in the oblate case; conversely, Monchiet et al. (2008)'s criterion was observed to be slightly more accurate in the prolate case. The comparisons with the isotropic criteria of Gurson (1977) and Gologanu et al. (1997), applying respectively to spherical and spheroidal voids, evidenced a coupling between plastic anisotropy and void shape: in all the cases considered, the two effects have comparable impacts upon the yield locus.

It is important to note that the numerical results obtained could also be used to validate any other macroscopic criterion for spheroidal voids embedded in an orthotropic Hill matrix.

This study validates the choice of velocity fields corresponding to an *isotropic* matrix in the derivation of the different models, even for *anisotropic* matrices. The good predictions of the anisotropic models based on "isotropic" velocity fields are in fact due to the variational characterization of the overall yield locus in terms of the overall plastic dissipation. This paves the way to a future extension of Madou and Leblond (2012a,b)'s recently proposed criterion for *general ellipsoidal* cavities embedded in an isotropic von Mises matrix, to the context of anisotropic Hill matrices: taking advantage of the previous remark, one may

hope to extend their criterion to anisotropic Hill matrices using again "isotropic" velocity fields.

References

Anderheggen, E., Knöpfel, H., 1972. Finite element limit analysis using linear programming. International Journal of Solids and Structures 8, 1413–1431.

Benzerga, A., 2000. Rupture ductile des tôles anisotropes. Ph.D. thesis. Ecole Nationale Supérieure des Mines de Paris, Paris, France.

Benzerga, A., Besson, J., 2001. Plastic potentials for anisotropic porous solids. European Journal of Mechanics-A/Solids 20, 397–434.

Bottero, A., Negre, R., Pastor, J., Turgeman, S., 1980. Finite element method and limit analysis theory for soil mechanics problems. Computer Methods in Applied Mechanics and Engineering 22, 131–149.

Capsoni, A., Corradi, L., 1997. A finite element formulation of the rigid–plastic limit analysis problem. International journal for numerical methods in engineering 40, 2063–2086.

Corradi, L., Luzzi, L., Vena, P., 2006. Finite element limit analysis of anisotropic structures. Computer methods in applied mechanics and engineering 195, 5422–5436.

De Borst, R., Feenstra, P.H., 1990. Studies in anisotropic plasticity with reference to the Hill criterion. Int. J. Numer. Meth. Engng. 29, 315–336.

Gologanu, M., 1997. Etude de quelques problèmes de rupture ductile des métaux. Ph.D. thesis. Université Pierre et Marie Curie (Paris VI)(in French).

Gologanu, M., Leblond, J., Devaux, J., 1993. Approximate models for ductile metals containing non-spherical voids–Case of axisymmetric prolate ellipsoidal cavities. Journal of the Mechanics and Physics of Solids 41, 1723–1754.

Gologanu, M., Leblond, J., Devaux, J., 1994. Approximate models for ductile metals containing non-spherical voids–Case of axisymmetric oblate ellipsoidal cavities. Journal of Engineering Materials and Technology 116, 290–297.

Gologanu, M., Leblond, J., Perrin, G., Devaux, J., 1997. Recent extensions of Gurson's model for porous ductile metals, in: Continuum Micromechanics, P. Suquet (Ed.), Springer-Verlag New York, pp. 61–130.

Gurson, A., 1977. Continuum theory of ductile rupture by void nucleation and growth: Part I-Yield criteria and flow rules for porous ductile media. Journal of Engineering Materials and Technology 99, 2–15.

Halphen, B., Nguyen, Q.S., 1975. Sur les matériaux standard généralisés. Journal de Mécanique 14, 39–63.

Hill, R., 1948. A theory of the yielding and plastic flow of anisotropic metals. Proceedings of the Royal Society of London, Series A, Mathematical and Physical Sciences 193, 281–297.

Hill, R., 1967. The essential structure of constitutive laws for metal composites and polycrystals. Journal of the Mechanics and Physics of Solids 15, 79–95.

Keralavarma, S., Benzerga, A., 2010. A constitutive model for plastically anisotropic solids with non-spherical voids. Journal of the Mechanics and Physics of Solids 58, 874–901.

Krabbenhoft, K., Damkilde, L., 2003. A general non-linear optimization algorithm for

lower bound limit analysis. International Journal for Numerical Methods in Engineering 56, 165–184.

Lee, B., Mear, M., 1992. Axisymmetric deformation of power-law solids containing a dilute concentration of aligned spheroidal voids. Journal of the Mechanics and Physics of Solids 40, 1805–1836.

Lyamin, A.V., Sloan, S., 2002a. Lower bound limit analysis using non-linear programming. International Journal for Numerical Methods in Engineering 55, 573–611.

Lyamin, A.V., Sloan, S., 2002b. Upper bound limit analysis using linear finite elements and non-linear programming. International Journal for Numerical and Analytical Methods in Geomechanics 26, 181–216.

Madou, K., Leblond, J.B., 2012a. A Gurson-type criterion for porous ductile solids containing arbitrary ellipsoidal voids–I: Limit-analysis of some representative cell. Journal of the Mechanics and Physics of Solids 60, 1020–1036.

Madou, K., Leblond, J.B., 2012b. A Gurson-type criterion for porous ductile solids containing arbitrary ellipsoidal voids–II: Determination of yield criterion parameters. Journal of the Mechanics and Physics of Solids 60, 1037–1058.

Madou, K., Leblond, J.B., 2013. Numerical studies of porous ductile materials containing arbitrary ellipsoidal voids-I: Yield surfaces of representative cells. European Journal of Mechanics-A/Solids , in press.

Mandel, J., 1964. Contribution théorique à l'étude de l'écrouissage et des lois de l'écoulement plastique, in: Proc. 11th Int. Congr. Appl. Mech, pp. 502–509.

Monchiet, V., Cazacu, O., Charkaluk, E., Kondo, D., 2008. Macroscopic yield criteria for plastic anisotropic materials containing spheroidal voids. International Journal of Plasticity 24, 1158–1189.

Monchiet, V., Charkaluk, E., Kondo, D., 2013. Macroscopic yield criteria for ductile materials containing spheroidal voids: an Eshelby-like velocity fields approach. Mechanics of Materials , in press.

Pastor, F., Pastor, J., Kondo, D., 2012. Limit analysis of hollow spheres or spheroids with hill orthotropic matrix. Comptes Rendus Mécanique 340, 120–129.

Sloan, S., 1988. Lower bound limit analysis using finite elements and linear programming. International Journal for Numerical and Analytical Methods in Geomechanics 12, 61–77.

Sloan, S., 1989. Upper bound limit analysis using finite elements and linear programming. International Journal for Numerical and Analytical Methods in Geomechanics 13, 263–282.

Sloan, S., Kleeman, P., 1995. Upper bound limit analysis using discontinuous velocity fields. Computer Methods in Applied Mechanics and Engineering 127, 293–314.

Son, N.Q., 1977. On the elastic plastic initial-boundary value problem and its numerical integration. International Journal for Numerical Methods in Engineering 11, 817–832.

A Summary of closed-form expressions of the criteria assessed

A.1 Macroscopic criterion for spherical voids (Benzerga and Besson)

Following Gurson (1977), the trial velocity field is of the form :

$$\underline{v} = \frac{\alpha}{r^2}\underline{e}_r + \boldsymbol{\beta}.\underline{x} \tag{A.1}$$

where $\boldsymbol{\beta}$ is a constant (uniform) second-order tensor and α is a constant.

The approximate yield criterion reads:

$$\left(\frac{\Sigma_{eq}}{\sigma_0}\right)^2 + 2f\cosh\left(\frac{\kappa\Sigma_h}{\sigma_0}\right) - 1 - f^2 = 0, \qquad \kappa = \frac{3}{2}\sqrt{\frac{5}{2h_1 + h_2 + 2h_3}} \tag{A.2}$$

The h_i here are connected to the coefficients of Hill's anisotropic tensor $\mathbb{H}$ as follows:

$$\begin{aligned} &h_1 = \frac{1}{4}(2H_{11} + 2H_{22} + 2H_{66} - H_{33}); \qquad h_2 = \frac{3}{2}H_{33}; \\ &h_3 = \frac{1}{2}(H_{44} + H_{55}) \end{aligned} \tag{A.3}$$

where $\mathbb{H}$ is defined by the condition: $\mathbb{H} : \mathbb{A} = \mathbb{A} : \mathbb{H} = \mathbb{K}$, $\mathbb{K}$ being the deviatoric projection tensor.

A.2 Macroscopic criterion for spheroidal voids (Monchiet et al.)

Following Gologanu et al. (1993, 1994), the trial velocity field $\underline{v}$ is of the form:

$$\underline{v} = \boldsymbol{A}.\underline{x} + B\underline{v}^E \tag{A.4}$$

where $\boldsymbol{A}$ is a constant (uniform) second-order tensor and B is a constant.

The approximate yield criterion reads:

$$\left(\frac{\widetilde{\Sigma}_{eq}}{\sigma_0}\right)^2 + 2(1+g)(f+g)\cosh\left(\frac{\kappa\Sigma_p}{\sigma_0}\right) - (1+g)^2 - (f+g)^2 = 0 \tag{A.5}$$

where :

$$\widetilde{\Sigma}_{eq}^2 = \Sigma_{eq}^2 + \frac{1}{1-h_2\zeta}\left(h_2\eta^2\Sigma_p^2 + \zeta\Sigma_q^2 + 2\eta\Sigma_p\Sigma_q\right) \tag{A.6}$$

The coefficients ζ and η are given by:

$$\eta = \frac{\kappa^2(1+g)(f+g)(\alpha_2-\alpha_1)}{(1-f)}; \quad \zeta = \frac{\kappa^2(1+g)(f+g)(\alpha_2-\alpha_1)^2}{(1-f)^2} \tag{A.7}$$

The expressions of Σ_q and Σ_p are:

$$\Sigma_q = \boldsymbol{\Sigma} : \boldsymbol{Q}; \quad \Sigma_p = \frac{1}{3}\boldsymbol{\Sigma} : \boldsymbol{X} \tag{A.8}$$

where $\boldsymbol{Q}$ is defined by:

$$\boldsymbol{Q} = \frac{1}{2}(\underline{e}_1 \otimes \underline{e}_1 + \underline{e}_2 \otimes \underline{e}_2) - \underline{e}_3 \otimes \underline{e}_3 \tag{A.9}$$

and $\boldsymbol{X}$ is given by:

$$\boldsymbol{X} = \frac{3}{2}(1-\alpha_2)(\underline{e}_1 \otimes \underline{e}_1 + \underline{e}_2 \otimes \underline{e}_2) + 3\alpha_2\ \underline{e}_3 \otimes \underline{e}_3 \tag{A.10}$$

The expression of κ is:

$$\kappa = \frac{3}{p} \tag{A.11}$$

where p is given by:

$$\begin{aligned} p^2 = \frac{3}{2}\frac{(1+g)(f+g)}{f(1-f)}\Big\{&(\beta_1 - f\beta_2)(h_1 + 3h_2 - 4h_3) \\ &+6\Big[\alpha_1(1-\alpha_1) - f\alpha_2(1-\alpha_2)\Big]h_2 + \Big[1-\alpha_1 - f(1-\alpha_2)\Big](h_1 - 3h_2 + 4h_3)\Big\} \end{aligned} \tag{A.12}$$

Coefficients h_i are defined by equations (A.3). The scalar functions α and β involved in the previous coefficients are defined by:

$$\begin{aligned} \alpha(e) &= \begin{cases} \dfrac{ab^2}{c^3}\text{argtanh}\left(\dfrac{c}{a}\right) - \dfrac{b^2}{c^2} & (\textit{prolate void}) \\ -\dfrac{ab^2}{c^3}\arctan\left(\dfrac{c}{a}\right) + \dfrac{b^2}{c^2} & (\textit{oblate void}) \end{cases} \\ \beta(e) &= \begin{cases} (1-3\alpha)\dfrac{a^2}{c^2} & (\textit{prolate void}) \\ -(1-3\alpha)\dfrac{a^2}{c^2} & (\textit{oblate void}) \end{cases} \end{aligned} \tag{A.13}$$

A.3 Macroscopic criterion for spheroidal voids (Keralavarma and Benzerga)

The expansion velocity field is taken to be axisymmetric about the void axis and constructed from the family of incompressible velocity fields introduced by Lee and Mear (1992). This corresponds to the fields used by Gologanu et al. (1997), which are a generalization of Gologanu et al. (1993, 1994)'s fields.

The approximate yield criterion is given by:

$$\begin{aligned}&\frac{3}{2}C\frac{\boldsymbol{\Sigma}:\mathbb{P}:\boldsymbol{\Sigma}}{\sigma_0^2}+2(1+g)(f+g)\cosh\left(\kappa\frac{\boldsymbol{\Sigma}:\boldsymbol{X}}{\sigma_0}\right)\\&-(1+g)^2-(f+g)^2=0\end{aligned}\tag{A.14}$$

where

$$\begin{aligned}&\mathbb{P}=\mathbb{A}+\eta(\boldsymbol{X}\otimes\boldsymbol{Q}+\boldsymbol{Q}\otimes\boldsymbol{X});\qquad \boldsymbol{Q}=\frac{1}{2}(\underline{e}_1\otimes\underline{e}_1+\underline{e}_2\otimes\underline{e}_2)+\underline{e}_3\otimes\underline{e}_3;\\&\boldsymbol{X}=\alpha_2(\underline{e}_1\otimes\underline{e}_1+\underline{e}_2\otimes\underline{e}_2)+(1-2\alpha_2)\ \underline{e}_3\otimes\underline{e}_3\end{aligned}\tag{A.15}$$

The expression of κ is:

$$\kappa=\begin{cases}\sqrt{3}\left\{\dfrac{1}{\ln f}\left[\dfrac{2}{3}\ln\dfrac{1-e_2^2}{1-e_1^2}+\dfrac{3+e_2^2}{3+e_2^4}-\dfrac{3+e_1^2}{3+e_1^4}+\dfrac{1}{\sqrt{3}}\left(\tan^{-1}\dfrac{e_2^2}{\sqrt{3}}-\tan^{-1}\dfrac{e_1^2}{\sqrt{3}}\right)\right.\right.\\\left.\left.-\dfrac{1}{2}\ln\dfrac{3+e_2^4}{3+e_1^4}\right]\dfrac{4\hat{h}_q+8\hat{h}_a-7\hat{h}_t}{10}+\dfrac{4(\hat{h}_q+2\hat{h}_a+2\hat{h}_t)}{15}\right\}^{1/2} & (prolate)\\\dfrac{3}{2}\left(\dfrac{\hat{h}_q+2\hat{h}_a+2\hat{h}_t}{5}\right)^{1/2}\left\{1+\dfrac{g_f-g_1+\frac{4}{5}(g_f^{5/2}-g_1^{5/2})-\frac{3}{5}(g_f^5-g_1^5)}{\ln\frac{g_f}{g_1}}\right\}^{-1} & (oblate)\end{cases}\tag{A.16}$$

where e_1 and e_2 are the eccentricities of the void and the outer boundary of the RVE[2]. The coefficients $\hat{h}_q$,$\hat{h}_t$ and $\hat{h}_a$ are defined by:

$$\begin{aligned}&\hat{h}_q=\frac{1}{6}(H_{11}+H_{22}+4H_{33}-4H_{23}-4H_{31}+2H_{12})\\&\hat{h}_t=h_1^{Monchiet};\qquad \hat{h}_a=h_3^{Monchiet}\end{aligned}\tag{A.17}$$

We define also the coefficients g, g_f and g_1 as:

[2] The void and the outer boundary are confocal.

$$
\begin{aligned}
&g = 0 \quad (prolate); \qquad g = \frac{e_2^3}{\sqrt{1-e_2^2}} \quad (oblate) \\
&g_f = \frac{g}{g+f}; \qquad g_1 = \frac{g}{g+1}
\end{aligned}
\tag{A.18}
$$

Finally the coefficient C involved in the quadratic form of the criterion reads:

$$
C = -\frac{2}{3}\frac{\kappa(g+1)(g+f)sh}{(Q^* + \frac{3}{2}\hat{h}_q \eta H^*)\eta}; \quad sh = \sinh(\kappa H^*); \quad ch = \cosh(\kappa H^*) \tag{A.19}
$$

where $H^* = 2\sqrt{\hat{h}_q}(\alpha_1 - \alpha_2)$ and $Q^* = 2\sqrt{\hat{h}_q}(1-f)$. The coefficient η reads:

$$
\eta = -\frac{2}{3\hat{h}_q}\frac{\kappa(g+1)(g+f)sh}{(g+1)^2 + (g+f)^2 + (g+1)(g+f)[\kappa H^* sh - 2ch]} \tag{A.20}
$$